MNRAS **000**, 1–12 (2016) Preprint December 20, 2016 Compiled using MNRAS LATEX style file v3.0

On the fragmentation boundary in magnetised self-gravitating discs

Duncan Forgan [1⋆], Daniel J. Price[2] and Ian Bonnell[1]
[1] *Scottish Universities Physics Alliance (SUPA), School of Physics and Astronomy, University of St Andrews, St Andrews KY16 9SS*
[2] *Monash Centre for Astrophysics (MoCA) and School of Physics and Astronomy, Monash University, Vic. 3800, Australia*

arXiv:1612.06145v1 [astro-ph.EP] 19 Dec 2016

Accepted

ABSTRACT

We investigate the role of magnetic fields in the fragmentation of self-gravitating discs using 3D global ideal magnetohydrodynamic simulations performed with the PHANTOM smoothed particle hydrodynamics code.

For initially toroidal fields, we find two regimes. In the first, where the cooling time is greater than five times the dynamical time, magnetic fields reduce spiral density wave amplitudes, which in turn suppresses fragmentation. This is the case even if the magnetic pressure is only a tenth of the thermal pressure. The second regime occurs when the cooling time is sufficiently short that magnetic fields cannot halt fragmentation.

We find that magnetised discs produce more massive fragments, due to both the additional pressure exerted by the magnetic field, and the additional angular momentum transport induced by Maxwell stresses. The fragments are confined to a narrower range of initial semimajor axes than those in unmagnetised discs. The orbital eccentricity and inclination distributions of unmagnetised and magnetised disc fragments are similar. Our results suggest the fragmentation boundary could be at cooling times a factor of two lower than predicted by purely hydrodynamical models.

Key words: accretion: accretion discs — stars: formation — quasars: supermassive black holes — planets and satellites: formation – magnetohydrodynamics (MHD)

1 INTRODUCTION

Self-gravitating accretion discs are expected to exist both around young stars and active galactic nuclei (AGN) (see e.g Kratter & Lodato 2016 and Rice 2016 for recent reviews). In star formation, the angular momentum distribution of dense molecular cloud cores (Goodman et al. 1993) ensures that upon collapse into star-disc systems, the discs have an initial mass comparable to the protostar (Lin & Pringle 1990; Bate 2010; Tsukamoto et al. 2014), ensuring that self-gravity plays a role in the disc evolution. Indeed, much of the star's final mass is expected to be drawn from the disc through efficient, globally determined angular momentum transport (Laughlin & Rozyczka 1996; Kratter et al. 2010; Forgan et al. 2011). In the case of AGN, the disc to central object mass ratio can be quite low (of order 10^{-3}) but may still be self-gravitating if the disc is thin (Goodman 2003; Lodato 2007).

Accretion discs are prone to the gravitational instability if (Toomre 1964)

$$Q = \frac{c_s \kappa}{\pi G \Sigma} \leq 1, \quad (1)$$

where c_s is the sound speed of the gas, Σ is the gas surface density. The quantity κ is the epicyclic frequency, which is equal to the angular frequency Ω if the disc is Keplerian. The 'Toomre Q' criterion (Eq. 1) refers to axisymmetric perturbations — non-axisymmetric perturbations are gravitationally unstable for $Q < 1.5$–1.7 (Durisen et al. 2007). Unstable non-axisymmetric perturbations develop into spiral density waves thanks to the differential rotation of the disc (Goldreich & Lynden-Bell 1965). These waves are trans-sonic, with Mach numbers of order unity (Cossins et al. 2009).

Depending on the available cooling mechanisms, the disc can become marginally stable (Paczynski 1978). This is a self-regulated quasi-steady state where Q is maintained near the stability limit, and the local weak shock heating through spiral density waves (increasing Q) approximately balances the local radiative cooling (reducing Q).

This quasi-steady state can be expressed in terms of the

⋆ E-mail:dhf3@st-andrews.ac.uk

© 2016 The Authors

dimensionless cooling parameter β_c, defined according to

$$\beta_c = t_{cool}\Omega, \tag{2}$$

where t_{cool} is the cooling time of the gas, and if the angular momentum transport is locally determined, by defining the dimensionless stress parameter α in terms of a pseudo-viscosity (Shakura & Sunyaev 1973; Gammie 2001):

$$\nu = \alpha c_s H, \tag{3}$$

where H is the disc scale height. This approximates the heating of the disc as due to a turbulent pseudo-viscosity. This is an acceptable approximation if the spiral density wave modes couple and decay into gravito-turbulence and $Q \sim 1$ (Balbus & Papaloizou 1999; Gammie 2001). When the disc is marginally stable and in thermal equilibrium, there is a direct relationship between this viscous stress heating and the radiative cooling, and thus

$$\alpha = \left|\frac{d\ln\Omega}{d\ln r}\right|^{-2}\frac{1}{\gamma(\gamma-1)\beta_c}, \tag{4}$$

where γ is the ratio of specific heats. If the radiative cooling is sufficiently vigorous (or the accretion of material into the disc is sufficiently vigorous), then this marginally stable state cannot be maintained. This has been interpreted as a maximum stress that the gravitational instability can support, with $\alpha_{\rm max} \approx 0.06$ (Rice et al. 2005). The gravitational stress saturates at this maximum value, and if density perturbations can continue to grow (either via strong cooling or rapid mass loading), then these perturbations become unstable to gravitational collapse, resulting in disc fragmentation.

There remains debate as to the precise value of this maximum (Meru & Bate 2011, 2012; Michael et al. 2012; Rice et al. 2012, 2014), and whether fragmentation can occur under low stresses, due to stochastic density fluctuations well above the RMS value that can occur given sufficient time (Paardekooper 2012; Young & Clarke 2015, 2016). It remains the case that fragmentation is *favoured* in discs that can no longer sustain thermal equilibrium through heating via spiral density waves and gravito-turbulence. Equivalently, disc fragmentation is favoured when the local Jeans mass inside a spiral density wave is decreasing rapidly (Forgan & Rice 2011), either through decreases in the local sound speed, or increases in the local gas density in the case of irradiated discs (Kratter & Murray-Clay 2011).

Magnetic fields have been absent from most studies of disc fragmentation to date. The usual argument for protostellar discs is that the low ionisation fractions mean that magnetic fields can be ignored. This is in stark contrast to studies of protostellar disc formation, which show that magnetic fields play a crucial role in extracting angular momentum from the system via magnetic braking. In ideal MHD simulations, this braking is so efficient that it can suppress disc formation entirely (Allen et al. 2003; Price & Bate 2007; Hennebelle & Ciardi 2009; Commerçon et al. 2010). Observations indicate that discs of order 100 au can exist around Class 0 protostars (e.g. Tobin et al. 2015), and the first direct observations of disc fragmentation proceed in this regime (Tobin et al. 2016). This apparent discrepancy between efficient magnetic braking and observed extended discs is resolved by either invoking turbulence, non-ideal MHD effects, or both (Seifried et al. 2013; Tomida et al. 2015; Wurster et al. 2016). Other surveys have shown that massive extended discs are perhaps less common (Maury et al. 2010), suggesting that some limited magnetic braking is occurring, and consequently limiting the frequency of disc fragmentation.

Discs around AGN are also likely to possess their own fields, through intense irradiation from the central engine and the surrounding environs. The presence of fields in both types of disc is evidenced by observations of jets and outflows, which are thought to be both launched and collimated by tightly wound field configurations (Pudritz et al. 2012; Marti-Vidal et al. 2015; Rodríguez-Kamenetzky et al. 2016).

There are few studies to date which consider the influence of magnetic fields on self-gravitating discs. During the same period that Gammie (2001) established equilibrium relationships for unmagnetised gravito-turbulence, Kim & Ostriker (2001) investigated magnetised self-gravitating gas in 2D shearing box simulations, determining that the magnetic Toomre Q

$$Q_m = \frac{\sqrt{c_s^2 + v_A^2}\,\Omega}{\pi G\Sigma} < 1.2 - 1.4, \tag{5}$$

for non-axisymmetric perturbations to grow in the presence of a magnetic field (see also Kim et al. 2003). Linear stability analysis of magnetised self-gravitating discs (Lin 2014) shows that the magneto-rotational instability (MRI) can be either stabilised or enhanced by gravitational instability (GI). If the resistivity is uniform, MRI modes with small radial lengths are stabilised. If the resistivity is a function of altitude from the midplane, MRI modes with radial length of order the disc thickness can be enhanced, which can significantly enhance axisymmetric density perturbations if the field is strong and toroidal. Interestingly, unstable modes can transition between MRI and GI, when the perturbations in gravitational potential and magnetic energy are comparable.

Fromang and collaborators (Fromang et al. 2004a,b; Fromang 2005) performed 3D global simulations (assuming an isothermal disc), which suggested that weak magnetic fields (with a plasma parameter $\beta_p \sim 10^3$) would not prevent fragmentation. The growth of MRI induces turbulence, creating spiral modes that are out of phase with those produced by GI, modulating the gravitational stress and subsequently the star's accretion rate. We will address here whether these features are due to the isothermal equation of state, or a generic feature of MRI-GI interaction in global discs.

More recently, local shearing box simulations were used to investigate the nature of 3D gravito-turbulence under the effect of weak ($\beta_p >> 1$) and strong fields ($\beta_p = 1$, Riols & Latter 2016). They identify three regimes, delineated by the energy balance between kinetic, gravitational and magnetic components. In the regime where magnetic energy is subdominant, a gravito-turbulent state can still be maintained, even with a relatively high Toomre-Q.

In the second regime, the magnetic energy exceeds the local gravitational energy (but not the kinetic energy). A gravito-turbulent state is still maintained, but the stresses in the system are now produced by magnetic fields, which use self-gravity as a dynamo. The weak turbulence maintained by gravitational instability is amplified by the formation of elongated current sheets, being dissipated as heat through magnetic reconnection. Interestingly, the deformation of the

field results in "plasmoids", magnetic islands which are remarkably similar to disc fragments, but created by fundamentally different physics. In the final regime, gravitational instability is completely suppressed by magnetic tension. Riols & Latter (2016) also studied the fragmentation boundary in the presence of magnetic fields. They find for a range of magnetic field strengths, the disc can still fragment if $\beta_c < 5$.

To date, there is no corresponding study of magnetic fields on disc fragmentation using 3D global simulations at sufficient resolution. To this end, we conduct a series of numerical experiments on magnetised self-gravitating accretion discs using smoothed particle hydrodynamics (SPH). We adopt a simple parametrisation to initialise both the local cooling rate and the initial magnetic field configuration, which we describe along with the code and our analysis methods in §2. In §3 we describe how magnetic fields alter the structure of self-gravitating discs and the properties of fragments that they produce. In §4 we discuss the implications of our results, and in §5 we summarise the work.

2 METHOD

2.1 Phantom

Smoothed Particle Hydrodynamics (SPH) is a Lagrangian method for solving the equations of fluid dynamics. The fluid is decomposed into a collection of particles, each possessing a mass m_i, position $\mathbf{r}_i$, velocity $\mathbf{v}_i$, internal energy u_i and smoothing length h_i (where i is the particle label). The density of the fluid at any position is reconstructed using the kernel weighted estimator

$$\rho(\mathbf{r}) = \sum_{i=1}^{N} m_i W(|\mathbf{r} - \mathbf{r}_i|, h), \tag{6}$$

where W is the smoothing kernel. The kernel function is selected to have compact support within the range $|\mathbf{r} - \mathbf{r}_i| = [0, 2h]$, so that N represents the number of neighbouring particles within a distance $2h$ of $\mathbf{r}$.

The equations of motion for the fluid proceed entirely from this density estimator (with an appropriate Lagrangian and variational principle), yielding a consistent framework for solving the (magneto)hydrodynamic equations (see Price 2012 for a review). We use the SPMHD code Phantom. The implementation of MHD in Phantom follows the basic scheme described in Price & Monaghan (2004a,b, 2005) (see review by Price 2012) with the divergence constraint on the magnetic field enforced using the constrained hyperbolic divergence cleaning algorithm described by Tricco & Price (2012) and Tricco et al. (2016). We assume ideal MHD for this work — the code is capable of non-ideal MHD (see e.g. Wurster et al. 2016) but this is beyond the scope of the present paper.

We employ artificial viscosity, conductivity and resistivity to resolve shocks and prevent unphysical particle interpenetration, for viscosity adopting the time-dependent viscosity of Morris & Monaghan (1997), where the α_{SPH} can vary between 0.1 and 1, and the corresponding non-linear viscosity term is fixed at $\beta_{SPH} = 2$. The particles evolve on individual timesteps, and the gravity forces are computed using a binary tree similar to that described in Gafton & Rosswog (2011).

The central object is represented by a sink particle (Bate et al. 1995), which accretes SPH particles which stray within a distance $r_{accrete}$, provided the SPH particle is bound and possesses an angular momentum less than that required to orbit beyond $r_{accrete}$. Particles that stray within $r_{accrete}/2$ are accreted without any checks. Dynamic sink creation is turned off, as our simulations can easily resolve the individual fragments (see section 3.1).

2.2 Calculating Disc Stresses

To compare the relative strength of self-gravity and magnetic fields in the steady state, we compute their associated stresses via the dimensionless α-parameter. This assumes that the angular momentum transport is locally determined, which is appropriate for self-gravitating discs when the disc to central object mass ratio is sufficiently low (Forgan et al. 2011). For each process, we compute the viscous stress tensor $T_{r\phi}$, which is related to α according to:

$$T_{r\phi} = \left| \frac{d \ln \Omega}{d \ln r} \right| \alpha \Sigma c_s^2, \tag{7}$$

i.e. T is proportional to the local pressure. Once T is computed, we simply invert for α using the vertically averaged sound speed and Σ. The viscous stress produced by gravito-turbulence can be written (Lynden-Bell & Kalnajs 1972)

$$T_{r\phi} = \int \frac{g_r g_\phi}{4\pi G} dz, \tag{8}$$

where g_r and g_ϕ are the radial and tangential components of the gravitational acceleration respectively. The Maxwell stress induced by the magnetic field is

$$T_{r\phi} = \int \frac{B_r B_\phi}{\mu_0} dz, \tag{9}$$

where again B_r and B_ϕ are radial and tangential field components. Finally, a third contribution to the total stress arises from the velocity and density perturbations produced by both the magnetic and gravitational fields - the Reynolds stress

$$T_{r\phi} = \Sigma \delta v_r \delta v_\phi, \tag{10}$$

where each δv represents deviations from the mean flow: e.g. $\delta v_r = v_r - \langle v_r \rangle$.

Artificial viscosity also induces angular momentum transport, and as such we should calculate it to confirm that our solutions are not dominated by numerics. This effective viscosity can be represented as (Artymowicz & Lubow 1994; Murray 1996; Lodato & Price 2010)

$$\nu_{\rm art} = \alpha_{\rm art} c_s H = \frac{1}{10} \alpha_{\rm AV} c_s h, \tag{11}$$

relating the user-defined artificial viscosity parameter α_{AV} to the resulting stress, represented by α_{art}

$$\alpha_{\rm art} = \frac{1}{10} \alpha_{\rm AV} \frac{< h >}{H}, \tag{12}$$

where $< h >$ is the azimuthally averaged smoothing length. As might be expected, discs with poorly resolved vertical structure will be dominated by artificial viscosity. As H decreases with decreasing r, the inner regions of our discs ($r \lesssim 7$) will be dominated by numerical viscosity.

2.3 CLUMPFIND analysis of Disc Fragments

We wish to identify how the properties of the fragments themselves change as the magnetic field is varied. We apply the CLUMPFIND algorithm to detect local minima in the gravitational potential (Smith et al. 2009). This algorithm places each particle into a clump depending on its gravitational potential ϕ, and that of the particles in its neighbour sphere.

The procedure is straightforward: All particles are sorted into a list of decreasing $|\phi|$, and are initially unassigned to any clumps. The sink particle representing the central star begins the first clump (along with its neighbour particles). The first particle on the list is then considered. If one of its neighbours is in clump j, then the particle is added to clump j. If the particle's neighbours belong to multiple clumps, then the particle is added to the clump to which the majority of its neighbours belongs. If the particle has no neighbours in a clump, it starts a new clump and adds its neighbours to it. We then move down the particle list to the next entry, and the process is repeated.

This procedure continues until all particles are tested. We have several choices in how we perform this analysis. As we wish to identify the smallest possible clumps, we do not include the contribution to the potential from the sink particle. If we had, then smaller potential wells would not be detected by the algorithm. Secondly, we do not stipulate that our clumps must be gravitationally bound (the basic CLUMPFIND algorithm is agnostic to a clump's boundness, but can be augmented to determine the bound component by removing outer particles until the clump's total energy is negative).

This gives a set of clumps for each timestep, but it does not inform us how to track a clump over several timesteps. To do this, we use a standard algorithm from halo tracking in cosmological simulations (cf Springel et al. 2001). For a clump i in timestep 1 and a clump j in timestep 2, the two clumps are shown to be the same clump if:

(i) The most bound particle in clump i is also in clump j, and
(ii) At least 50% of the particles in clump i are also in clump j

We can then use this clump tracking system to measure mass evolution of the fragment, as well as orbital data.

3 RESULTS

3.1 Initial Conditions

We adopt initial conditions similar to those employed by Rice et al. (2005) and many subsequent authors. The simulations are scale-free. The disc is composed of N_{part} SPH (gas) particles, with a surface density profile $\Sigma \propto r^{-1}$, sound speed profile $c_s \propto r^{-0.75}$, extending between $r_{in} = 0.25$ and $r_{out} = 25$, with a total mass $M_d = 0.25$. The central object is represented by with a sink particle, mass $M = 1$, placed initially at the origin. The sink is free to move, with $r_{accrete} = 0.25$.

We assume an adiabatic equation of state, with the ratio of specific heats $\gamma = 5/3$. We adopt the usual β-cooling formalism

$$\dot{u}_{\rm cool} = -\frac{u}{t_{\rm cool}} = -\frac{u\Omega}{\beta_c}, \tag{13}$$

where we fix $\beta_c = $ const. throughout the disc. We initialise a toroidal magnetic field with strength given by a plasma parameter β_p which is initially constant with radius

$$\beta_p = \frac{2P\mu_0}{B^2}, \tag{14}$$

i.e., the ratio of thermal to magnetic pressure. The magnetic field is allowed to evolve freely under ideal MHD conditions, with no external field applied.

To resolve fragmentation correctly, we must ensure that the Jeans mass is larger than a neighbour-group of particles (Bate & Burkert 1997), i.e.

$$M_{J,\rm resolve} = 2M_d \frac{N_{\rm neigh}}{N_{\rm part}}. \tag{15}$$

For our simulations, the minimum Jeans mass resolvable is $M_{J,\rm resolve} = 5 \times 10^{-5}$ for $N_{\rm part} = 5 \times 10^5$, and $M_{J,\rm resolve} = 2.5 \times 10^{-6}$ for $N_{\rm part} = 10^6$. As we will see in the following sections, the typical fragment mass is of order 10^{-3}, which is well above the resolution limit.

This resolution is only guaranteed to be sufficient where the disc evolution is also well resolved, i.e. where the artificial viscosity in the simulation is low compared to the pseudo-viscosity generated by the gravitational and magnetic fields, as described in section 2.2. If not, self-gravitating fragments may not form due to excessive artificial angular momentum transport.

3.2 Steady State Discs

Before assessing fragmenting systems, we perform two calculations with $N_{\rm part} = 10^6$ and $\beta_c = 9$ to investigate the steady-state behaviour of non-fragmenting self-gravitating discs with and without magnetic fields. Visually inspecting both discs at the same timestep (Figure 1), it is immediately obvious that magnetic fields attenuate the gravitational instability in the outer region. The mean column density structure appears to be similar in both cases, but the spiral density waves present throughout the unmagnetised disc are suppressed in the magnetised disc at $r > 15$.

We can confirm this by inspecting the time-averaged surface density and Toomre Q parameter (Figure 2). Adding a toroidal field (with strength given by $\beta_p = 10$) does not significantly affect the surface density profile between $r = 5 - 20$, but does result in a more shallow profile beyond $r = 20$. The sound speed in the disc increases noticeably beyond $r = 10$ (where Maxwell stresses begin to become significant, see Figure 3). As the rotation curves of both discs are very similar, the resulting Toomre Q for the magnetised disc increases sharply beyond $r = 15$. If one considers the magnetic Toomre Q parameter

$$Q_m = \frac{\sqrt{c_s^2 + v_A^2}\Omega}{\pi G \Sigma} = Q\sqrt{1 + \frac{1}{\beta_p}}, \tag{16}$$

a gravitationally unstable magnetised disc would still possess a standard Toomre Q close to 1.5-2 for $\beta_p = 10$. The magnetic stresses have therefore caused sufficient heating to

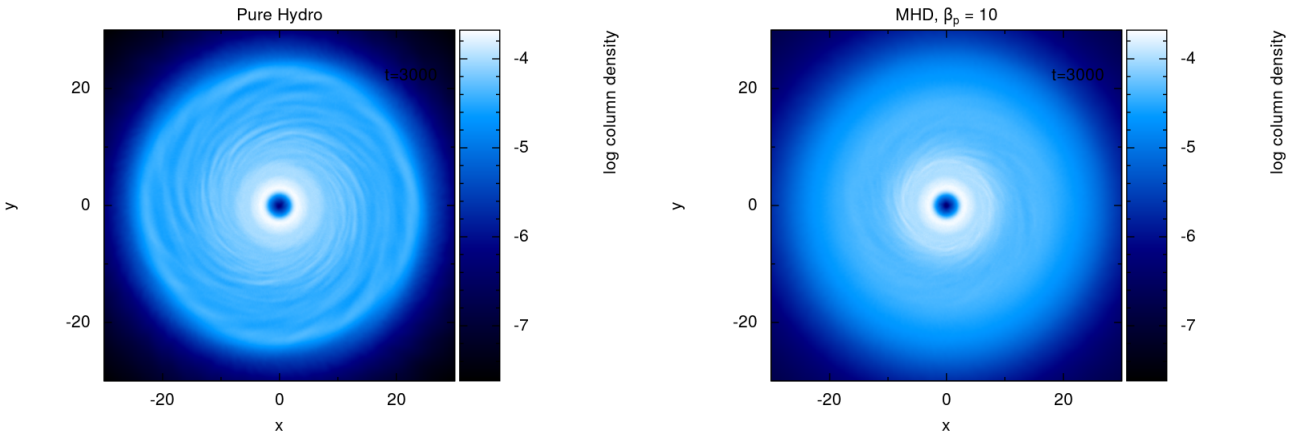

Figure 1. Comparison of surface density between the unmagnetised (left) and magnetised (right; with $\beta_p = 10$) calculations, using $\beta_c = 9$. The disc is smoother, with weaker spiral shocks in the magnetised case

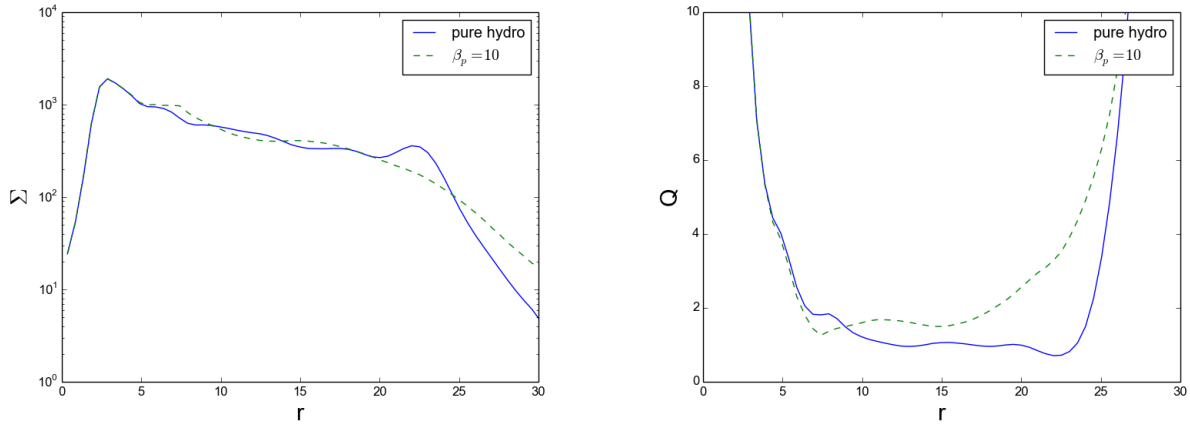

Figure 2. Comparison of steady state disc structures in non-fragmenting self-gravitating discs. We show time-averaged surface densities (left) and time averaged Toomre Q parameter (right) in the magnetised (dashed line) and unmagnetised (solid line) cases.

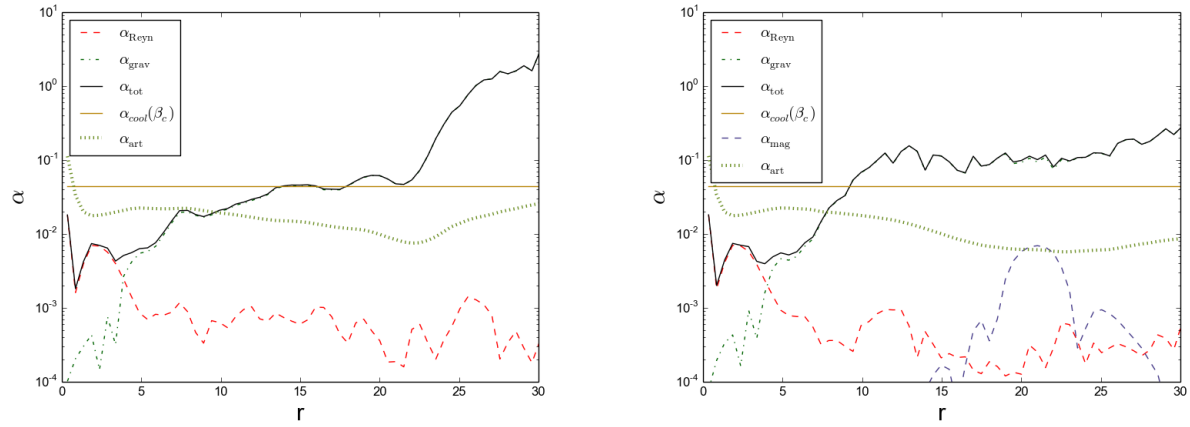

Figure 3. Angular momentum transport in non-fragmenting self-gravitating discs. Left panel shows the time-averaged α-parameters for an unmagnetised disc with $\beta_c = 9$, while right panel shows the same disc with $\beta_c = 9$ and $\beta_p = 10$. In both cases we also plot the predicted $\alpha(\beta_c)$ for an unmagnetised self-gravitating disc in thermal equilibrium.

outmatch the local β_c-cooling, and quell the gravitational instability in this disc.

This is also reflected in the measured angular momentum transport (Figure 3). We plot the α-parameter for each component, and the total

$$\alpha_{\rm tot} = \alpha_{\rm Reyn} + \alpha_{\rm grav} + \alpha_{\rm mag}. \quad (17)$$

We also plot the predicted total α, $\alpha_{\rm cool}$ given $\beta_c = 9$ and $\gamma = 5/3$ (for an unmagnetised disc)

$$\alpha_{\rm cool}(\beta_c) = \frac{4}{9\gamma(\gamma-1)\beta_c} = 0.0444. \quad (18)$$

The unmagnetised disc (left plot in Figure 3) possesses an $\alpha_{\rm tot}$ close to that of the predicted value between $r \sim 12 - 22$, which corresponds neatly to the minima in Q demonstrated in the right panel of Figure 2. In the magnetised case, the disc exhibits a total $\alpha \sim 0.1$, quite in excess of the unmagnetised prediction. However, we can see that this is not due to the significant increase of adding a non-zero $\alpha_{\rm mag}$, or an enhanced $\alpha_{\rm Reyn}$. In fact, there are indications that $\alpha_{\rm Reyn}$ is decreased compared to the unmagnetised case, presumably due to weaker spiral density wave structures failing to generate the same strength of velocity perturbations.

The increased total stress must be purely from gravitational forces, and appears to be due to the modified disc structure produced by adding magnetic fields. The magnetised disc maintains a shallower surface density profile, and hence the gravitational torques exerted by the outer disc become more significant in the inner parts. Large scale magnetic fields are also likely to be mediating torques and boosting stresses. These fields are also producing weak outflows, resulting in a negligible amount of mass at high altitude compared to the unmagnetised case.

The Toomre-Q in these regions remains approximately 2 and larger, ensuring that the disc is stable against gravitational perturbations, even when the gravitational stresses remain high. We should therefore view this enhanced stress as resulting from long-range torques from the outer disc, rather than locally generated gravito-turbulence. As long-range torques can generate α values well in excess of the fragmentation boundary without producing fragments (cf Harsono et al. 2011), the disc can remain stable under such perturbations.

3.3 Fragmenting Discs

If we now reduce the cooling time into the fragmentation regime, such that $\beta_c = 4$, we might expect the outer regions of the disc to remain stable against fragmentation. Once more, visual comparison of unmagnetised and magnetised fragmenting discs confirms this hypothesis (Figure 4). Both discs have a low $\beta_c = 4$. The unmagnetised disc (left) fragments promptly, at all radii where Q reaches the marginally stable regime. The same is true for the magnetised disc, but the outer regions are no longer in the marginally stable regime, as Q increases above 2 beyond $r \sim 15$, in a manner similar to the stable magnetised disc presented in section 3.2 (see Figure 2).

And what of the fragments themselves? We use the CLUMPFIND algorithm to study the properties of the fragments produced. Figure 5 shows the mass distribution of fragments as a function of simulation time. In the unmagnetised case, short-lived fragments initially form with masses in the range $m = 0.001$–0.004 (if the mass is given to be in Solar units, this is approximately 1–4 Jupiter masses). Fragments above $m = 0.001$ are more persistent, surviving several orbits before migrating inwards to be tidally disrupted. When the initial plasma $\beta_p = 10$, the number of fragments produced is significantly lower. The masses of these fragments is also somewhat larger, extending towards $m = 0.006$–0.008. This is due to an effective increase in the Jeans mass in the presence of the magnetic field, and the global redistribution of disc material due to Maxwell stresses (see Discussion).

The semimajor axis distribution of the fragments reflects the regions of the disc that remain gravitationally unstable (top row of Figure 6). The unmagnetised disc is unstable from around $r = 5$ to its maximum extent, and fragments promptly from around $r = 10$ outwards to $r = 20$. The magnetised disc is constrained to fragment within a narrower radius limit, as the outer disc cannot maintain a sufficiently low Q to permit fragmentation.

In both cases, the orbital eccentricities of the fragments are typically low (middle row of Figure 6), and the underlying distribution is similar for both unmagnetised and magnetised discs. Individual fragment tracking shows that the eccentricity of fragments tends to increase with time (as semimajor axis decreases). This is presumably due to interactions with other fragments and the local disc structure extracting angular momentum and allowing inward migration towards tidal disruption.

Most fragments form very close to the orbital plane, whether magnetic fields are active or otherwise (bottom row of Figure 6). Again, the inclination distribution appears to be insensitive to the magnetic field, with the majority of all fragments forming within 0.2° of the disc midplane.

3.4 Magnetic Fields as a Fragmentation Suppressor

Imposing strong magnetic fields can suppress fragmentation if the cooling time is sufficiently long, for example if we set $\beta_c = 5$, $\beta_p = 1$. Visual inspection of the surface density structure compared to the unmagnetised control run (Figure 7) shows that spiral structures can still exist in the inner disc. The outer disc is extremely smooth, with no signs of fragmentation.

The Toomre-Q parameter confirms that only the inner radii ($r = 5 - 15$) can be considered to be gravitationally unstable (left panel of Figure 8). The gravitational stress dominates angular momentum transport, and far exceeds the value predicted by local equilibrium. Despite this, the disc does not fragment. The magnetic field does not appear to be strong enough in this regime to prevent fragmentation, but it may be the case that the stable outer disc is generating strong torques in the inner disc, invalidating the local transport approximation.

If we now look beyond $r = 15$, the Maxwell stress increases, causing significant heating (right panel of Figure 8). Interestingly, the disc maintains a total α that is close to the value predicted by local thermodynamic equilibrium for our imposed β_c, suggesting that angular momentum transport is still being mediated by turbulent pseudo-viscosity, where the turbulence is generated by (roughly equal) gravitational and

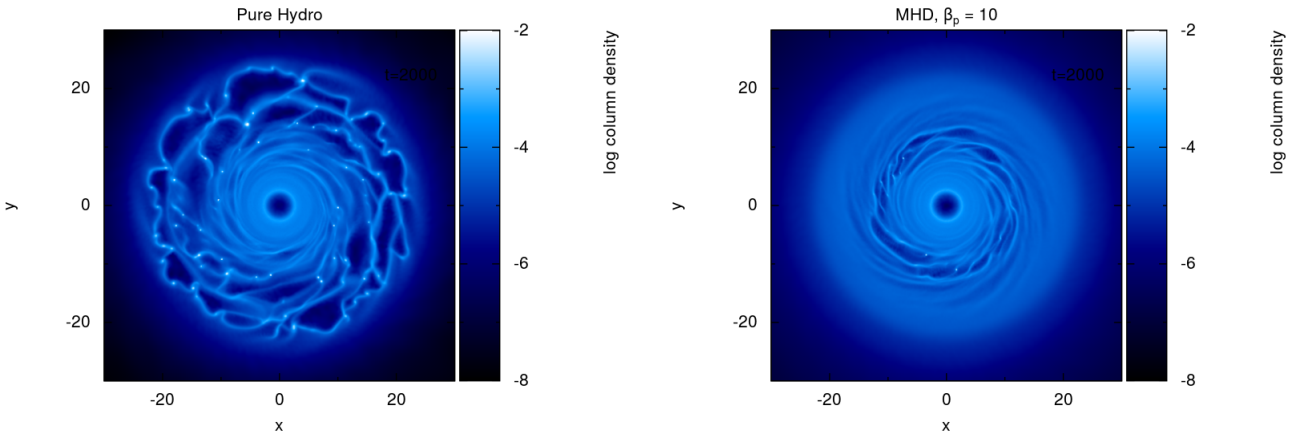

Figure 4. Comparison of fragmentation in unmagnetised (left) and magnetised (right; $\beta_p = 10$) discs. Both plots have a $\beta_c = 4$ and $N_{\rm part} = 5 \times 10^5$ and are shown at $t = 2000$.

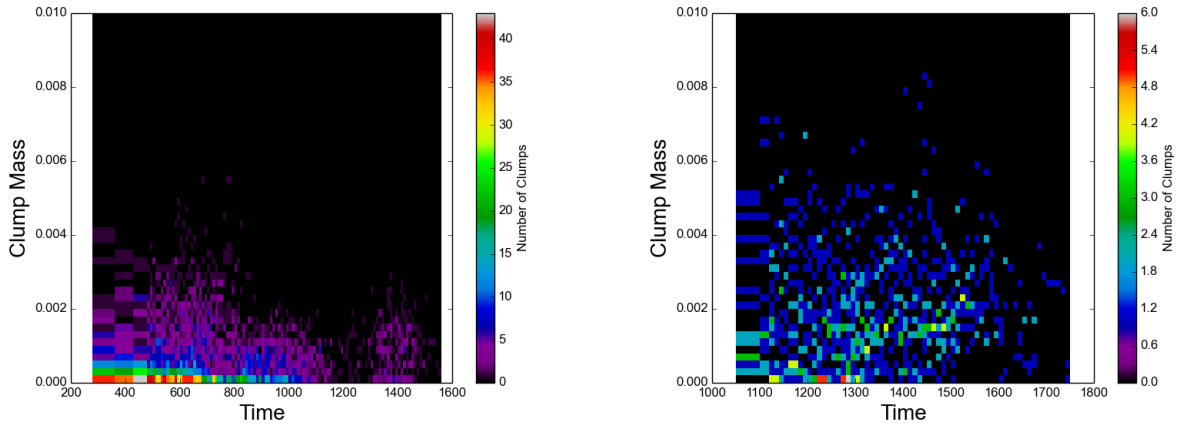

Figure 5. Distribution of fragment mass as a function of time, for simulations with $\beta_c = 4$, $N_{part} = 10^6$. Left shows the unmagnetised case, and right the $\beta_p = 10$ case

magnetic stresses. The gravitational stress in this regime is $\sim 0.05 - 0.06$ - in the absence of a magnetic field, the total α would lie just below the critical value for fragmentation. This indicates that magnetic fields suppress disc fragmentation by reducing gravitational stresses, as found by both local and global simulations (Fromang 2005; Riols & Latter 2016).

3.5 The Fragmentation Boundary for Magnetised Discs

Finally, we investigate the propensity of discs to fragment as a function of (β_c, β_p). Figure 9 shows the resulting behaviour of discs in this parameter space, at two different resolutions: $N_{part} = 5 \times 10^5, 10^6$. Note that without magnetic fields, all of the discs studied fragment promptly.

Addition of magnetic fields at $\beta_c = 5$ completely suppresses fragmentation, even at $\beta_p = 10$. This is in accordance with the results of the previous section, which indicate that magnetic fields reduce the gravitational stress in the outer disc below the limit required for prompt fragmentation, and increase Q. Given that in the strongest field scenario, the gravitational stress for a $\beta_c = 5$ disc is about 0.05 (Figure 8), with the prompt fragmentation boundary for unmagnetised discs lying close to $\alpha = 0.06$ (Rice et al. 2005), it seems reasonable that a slight decrease in β_c from 5 to 4 would be sufficient to raise the gravitational stress so that the total α exceeds the fragmentation limit.

4 DISCUSSION

Our principal result — that magnetic fields can suppress fragmentation for cooling times above five times the dynamical time— is in broad agreement with the local simulations conducted by Riols & Latter (2016). They also show fragmentation is suppressed for $\beta_p = 8$ if $\beta_c > 5$. We should however note that global and local simulations must be compared carefully. Our global simulations show fragmentation suppression due not only to direct action of the magnetic

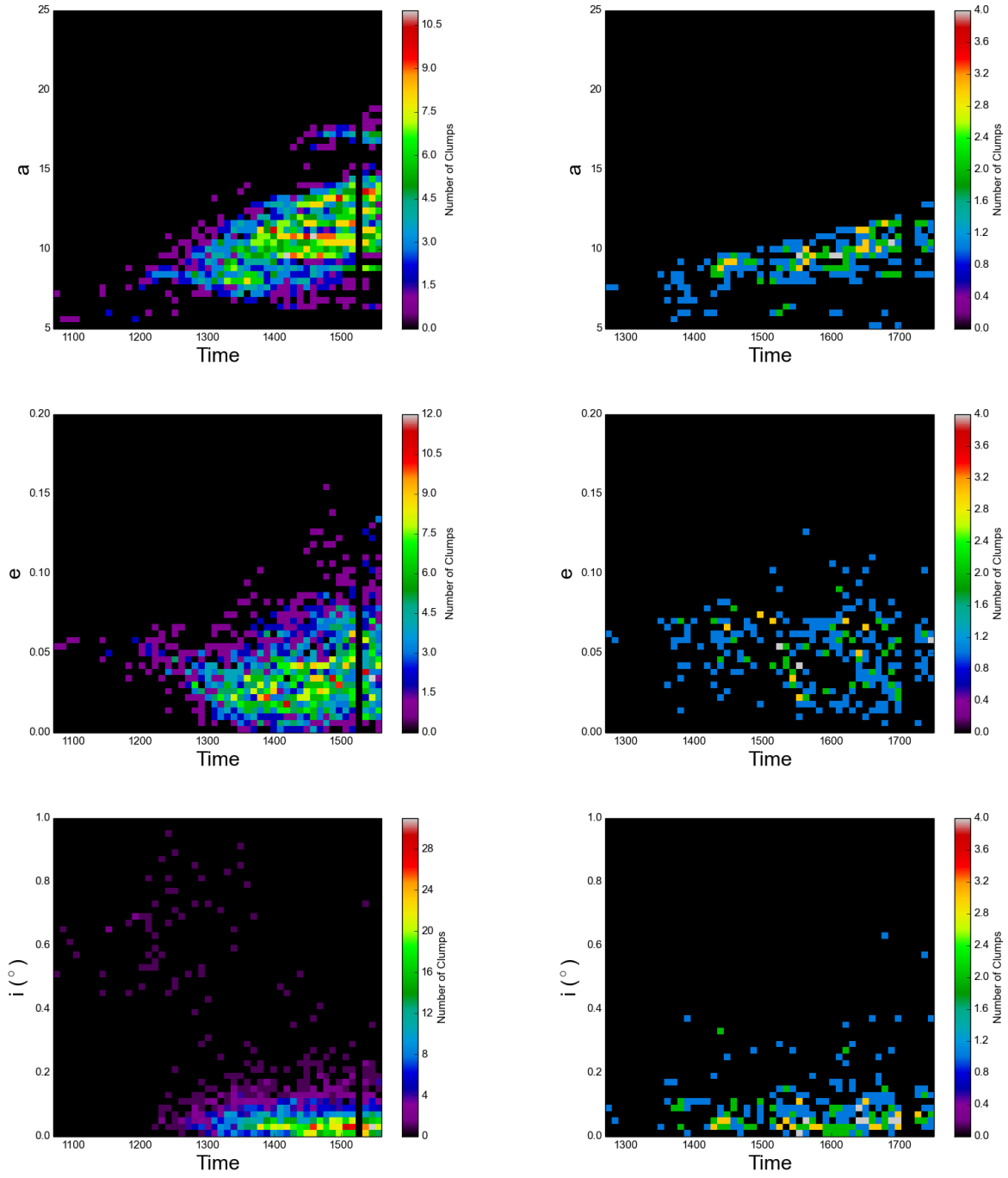

Figure 6. The distribution of fragment orbital elements as a function of time,for simulations with $\beta_c = 4$, $N_{part} = 10^6$. The left column shows the unmagnetised case, and the right the $\beta_p = 10$ case. Top row: semi-major axis, middle row: eccentricity, bottom row, orbital inclination.

field, but also to redistribution of the disc material diluting the gravitational instability. Local simulations typically strictly conserve mass within the domain of interest, in effect preventing global redistribution of mass and energy as we observe.

What values of β_p might we expect in real discs? Wurster et al. (2016) report values between 10-1000, from the inner and outer disc respectively. This is true both for their ideal and non-ideal MHD simulations of protostellar disc formation, and appears to be confirmed by other work (e.g. Tomida et al. 2015). This would suggest that disc fragmentation is not prevented by magnetic fields, provided the disc cooling rate is sufficiently strong locally. If the system retains enough angular momentum to form an extended disc, this seems quite possible (Forgan & Rice 2012).

This suppression of fragmentation at what is quite low

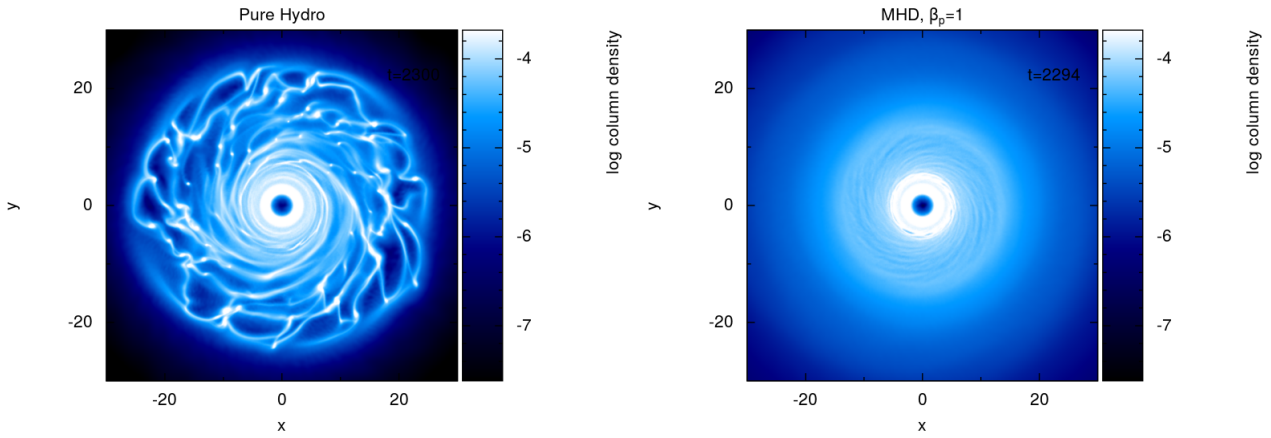

Figure 7. Suppression of fragmentation in strongly magnetised discs (comparing left and right panels), showing the calculations with $N_{\rm part} = 10^6$ and $\beta_c = 5$. The left is unmagnetised, the right has a strong magnetic field ($\beta_p = 1$). While non-axisymmetric structure is evident in the form of spiral density waves, these waves have a small perturbation amplitude and do not fragment.

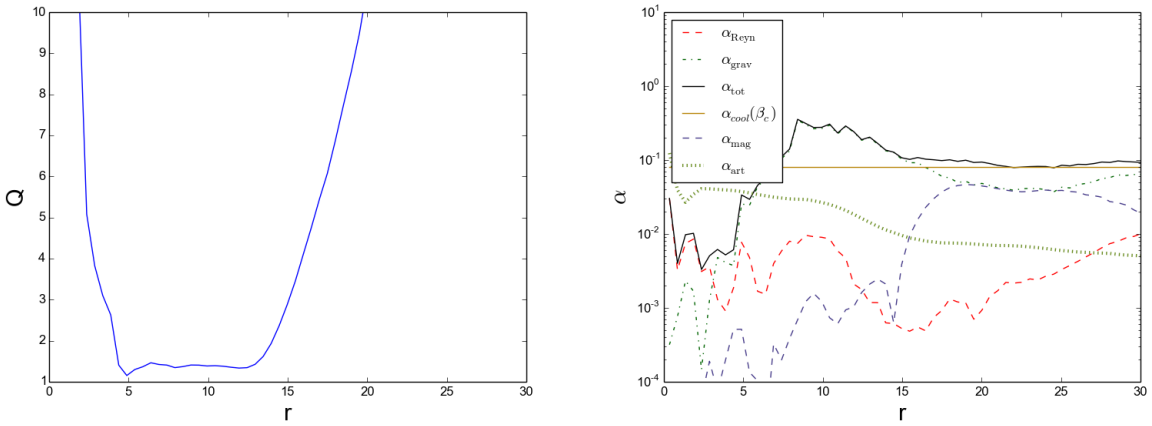

Figure 8. Toomre-Q profile (left) and angular momentum transport parameters (right) in the strongly magnetised case ($\beta_c = 5$, $\beta_p = 1$). The outer regions of the disc are too hot to be gravitationally unstable. The disc maintains local thermodynamic equilibrium by equipartion of gravitational and magnetic stresses. .

β_c, by typical values of β_p, is important to considerations of convergence in unmagnetised simulations. If the boundary for prompt fragmentation is $\beta_c \sim 7-8$ for zero field, and potentially higher for stochastic fragmentation, then the addition of what is quite a weak field reduces the critical β_c significantly, and requires quite strong cooling for fragmentation to occur at all. This suggests that discussions of whether the prompt fragmentation boundary truly is $\beta_c = 7, 8$ or even 9 might not be particularly relevant to real self-gravitating discs, even if their magnetic fields are weak.

Our simulations indicate that there is both a minimum and maximum radius for fragmentation to occur when magnetic fields are active, but we should note that this could be an artifact of our idealised cooling. As β_c declines with radius in realistic protostellar discs, we should therefore expect fragmentation to be further restricted to regions where β_c is very low and Q is maintained at the marginal stability limit, i.e. radii beyond 30 au. Further work is required to show whether there is a maximum radius for disc fragmentation, which will depend on the equilibrium disc structure produced by magnetised self-gravitating discs with realistic thermodynamics.

Our increased fragment masses are expected from analytic calculations of the magnetic Jeans mass (Strittmatter 1966). For a medium with a uniform field along a single axis, a density perturbation will only be resisted along the two axes perpendicular to the field vector. The Jeans length λ_J along these axes is modified thus (Chandrasekhar & Fermi 1953):

$$\lambda^2_{J,mag} = \lambda^2_J \left(1 + \frac{v^2_A}{c^2_s}\right) = \lambda^2_J \left(1 + \frac{1}{\beta_p}\right) \qquad (19)$$

However, a perturbation of Jeans mass $M_J \propto \rho\lambda_{\rm J}\lambda^2_{\rm J,mag}$ will be insufficient to contract along the magnetic field lines - indeed, a Jeans mass $M_J \propto \rho\lambda^3_{\rm J,mag}$ is needed. This back-

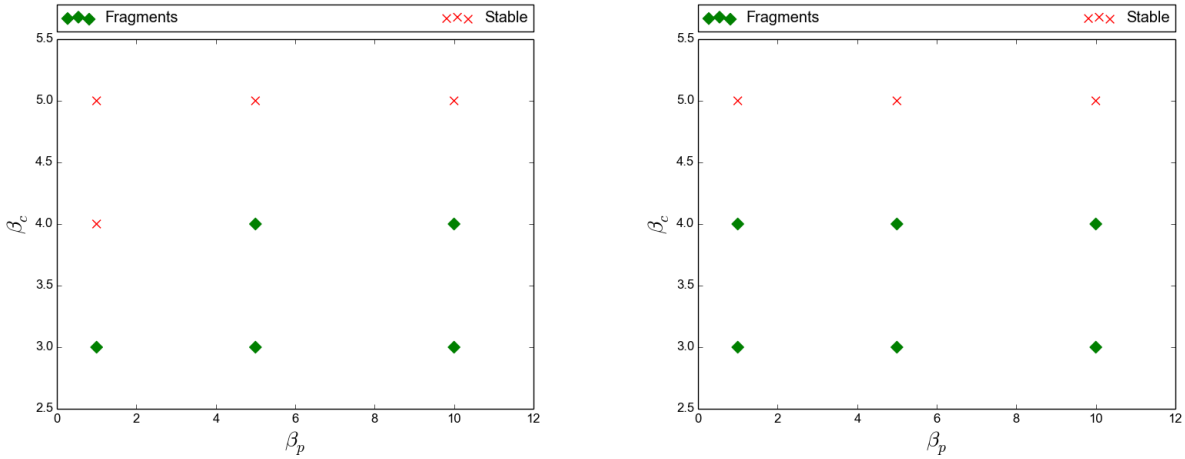

Figure 9. The fragmentation boundary in magnetised self-gravitating discs. Left panels shows results from calculations with $N_{\rm part} = 5 \times 10^5$, while right panels shows results with $N_{part} = 10^6$. Note the change in status for runs with $\beta_c = 4$, $\beta_p = 1$. All of the above simulations fragment in the absence of magnetic fields.

of-the-envelope calculation suggests we should expect an increase in fragment mass by a factor of $\left(1 + \frac{1}{\beta_p}\right)^{3/2}$ - between $1.1^{3/2}$ to $2\sqrt{2}$. We do indeed see that our maximum fragment mass increases by a factor of 2. Applying the converse calculation suggests that $\beta_p \approx 1.7$ in the most massive fragments (when the disc was initialised with $\beta_p = 10$).

A more accurate estimate of the fragment mass should consider the properties of the disc material inside a spiral density wave (Forgan & Rice 2011). Future studies of expected initial fragment mass should consider the impact of magnetic fields in this manner.

We should be careful about extrapolating fragment behaviour from numerical experiments like this - the fragments are interacting with a disc structure unlikely to exist in real discs. In practice, we expect β_c to increase with increasing proximity to the star, as the cooling time of the gas increases with increasing Σ. This being said, we do see rapid inward migration, which is a common feature of fragments in self-gravitating discs, not only due to the increased torques exerted on the fragment from a more massive disc (Baruteau et al. 2011), but also the fragment's inability to open a gap and enter the slower Type II migration mode (Malik et al. 2015). We recommend CLUMPFIND analysis techniques be applied to simulations of fragmenting discs with realistic thermodynamics to investigate the dynamical properties of fragments further (see e.g. Hall et al, in prep).

Of particular importance to fragment survival is the evolution of spin angular momentum. Kim et al. (2003), in their study of giant molecular cloud formation in magnetised galactic discs, noted that the GMCs formed in the disc were subject to strong magnetic braking, losing a significant portion of their initial spin angular momentum. In fragments, this will have important consequences for the discs they may host (Forgan 2016). It will also affect the fragment's ability to collapse into bound objects, preventing Roche lobe overflow and tidal disruption (cf Boley & Durisen 2010; Nayakshin 2010; Zhu et al. 2012; Forgan & Rice 2013).

We must note that none of our simulations resolve the magneto-rotational instability (MRI). In protostellar discs, this instability primarily acts in the inner disc, most especially in regions where artificial viscosity dominates our simulations. In the case of a global SPH disc simulation, we find that resolving the MRI is equivalent to another vertical resolution criterion, which in practice is computationally prohibitive. For the fastest growing MRI mode to be resolved, we must satisfy:

$$\frac{h}{H} < 2\pi\sqrt{\frac{16}{15\beta_p}} \tag{20}$$

We do not satisfy this condition anywhere in our discs, even for relatively large β_p. As a result, we only resolve a fraction of the MRI modes present, and our description of the magnetic turbulence is incomplete. We therefore cannot comment on the possible interaction between MRI and GI, in particular whether GI modes can encourage the activation of MRI in the inner disc, which semi-analytic models predict sustains a limit cycle of episodic accretion (Armitage et al. 2001; Martin & Lubow 2014). Conversely, simulations have already indicated that MRI modes can weaken the gravitational instability and prevent collapse (Fromang 2005; Riols & Latter 2016), in much the same way that fragmentation has been suppressed in our simulations. The fact that we find qualitative agreement with studies that fully resolve the MRI suggests that our results regarding disc fragmentation are robust.

Finally, we should acknowledge the critical role that non-ideal MHD effects may play in self-gravitating discs, especially in the coupling of gas and dust grains. Spiral density waves in unmagnetised discs have been shown to collect centimetre-metre size grains, in some cases showing significant overdensities (Rice et al. 2004; Dipierro et al. 2015). Whether such overdensities should be expected in observations of self-gravitating discs depends on the ability of grains to grow to sizes such that the Stokes number is of order unity. This in turn requires the velocity dispersion of the grains to remain sufficiently low during growth, which tends to restrict this effect to large radii (Booth & Clarke 2016). This is where magnetic fields are most efficient at

reducing gravitational stresses and spiral perturbation amplitudes, so magnetic fields may also suppress grain growth in self-gravitating discs.

Depending on the grain charge, non-ideal effects are likely to play an important role in mediating the separation of the gas and dust phases. In particular, Ohmic heating is likely to alter the structure of the spiral density wave and the weak shocks it induces.

5 CONCLUSIONS

We have conducted a series of numerical experiments on magnetised self-gravitating discs using the smoothed particle magnetohydrodynamics code PHANTOM, to test the effects of magnetic fields on disc fragmentation. We parametrise the disc thermodynamics by fixing the cooling time relative to the dynamical time (β_c), and we initially impose a purely toroidal magnetic field, where the field strength is set as a constant plasma parameter β_p, i.e. the magnetic pressure is initially a fixed fraction of the thermal pressure.

We select sufficiently small values of β_c that fragmentation occurs for all our discs in the absence of magnetic fields. We find that fragmentation in magnetised protostellar discs can still occur provided $\beta_c < 5$, for both weak and strong fields (i.e. $\beta_p = 1$). For $\beta_c = 5$, fragmentation can be suppressed even by relatively weak fields ($\beta_p = 10$).

Discs that fragment in the presence of magnetic fields produce fragments of increased mass compared to unmagnetised discs. Their orbital eccentricity and inclination are very similar to unmagnetised fragments, although our simulations show that there may be a minimum and maximum radius at which fragmentation occurs, as opposed to merely a minimum for unmagnetised discs.

We recommend that future studies of disc fragmentation must consider even weak magnetic fields, as they are likely to push the fragmentation zone even further from the central object, with obvious implications for planet/brown dwarf formation in protostellar discs, and star formation in discs around active galactic nuclei.

ACKNOWLEDGMENTS

DHF and IAB gratefully acknowledge support from the ECOGAL project, grant agreement 291227, funded by the European Research Council under ERC-2011-ADG. DJP gratefully acknowledges funding via grants DP130102078 and FT130100034 and via Future Fellowship FT130100034 from the Australian Research Council. This work relied on the compute resources of the St Andrews MHD Cluster. Surface density plots were created using SPLASH (Price 2007).

References

Allen A., Li Z., Shu F. H., 2003, ApJ, 599, 363
Armitage P. J., Livio M., Pringle J. E., 2001, MNRAS, 324, 705
Artymowicz P., Lubow S. H., 1994, ApJ, 421, 651
Balbus S. A., Papaloizou J., 1999, ApJ, 521, 650
Baruteau C., Meru F., Paardekooper S.-J., 2011, MNRAS, 416, 1971
Bate M. R., 2010, MNRAS, 404, L79
Bate M. R., Burkert A., 1997, MNRAS, 288, 1060
Bate M. R., Bonnell I. A., Price N., 1995, MNRAS, 277, 362
Boley A. C., Durisen R. H., 2010, ApJ, 724, 618
Booth R. A., Clarke C. J., 2016, Monthly Notices of the Royal Astronomical Society, 458, 2676
Chandrasekhar S., Fermi E., 1953, The Astrophysical Journal, 118, 116
Commerçon B., Hennebelle P., Audit E., Chabrier G., Teyssier R., 2010, Astronomy and Astrophysics, 510, L3
Cossins P., Lodato G., Clarke C. J., 2009, MNRAS, 393, 1157
Dipierro G., Pinilla P., Lodato G., Testi L., 2015, MNRAS, 451, 974
Durisen R., Boss A., Mayer L., Nelson A., Quinn T., Rice W. K. M., 2007, in Reipurth B., Jewitt D., Keil K., eds, Protostars and Planets V. University of Arizona Press, pp 607–622
Forgan D., 2016, ArXiv e-print:1602.06713, submitted to the Open Journal of Astrophysics
Forgan D., Rice K., 2011, MNRAS, 417, 1928
Forgan D., Rice K., 2012, MNRAS, 420, 299
Forgan D., Rice K., 2013, MNRAS, 432, 3168
Forgan D., Rice K., Cossins P., Lodato G., 2011, MNRAS, 410, 994
Fromang S., 2005, A&A, 441, 1
Fromang S., Balbus S. A., De Villiers J.-P., 2004a, ApJ, 616, 357
Fromang S., Balbus S. A., Terquem C., De Villiers J.-P., 2004b, ApJ, 616, 364
Gafton E., Rosswog S., 2011, MNRAS, 418, 770
Gammie C., 2001, ApJ, 553, 174
Goldreich P., Lynden-Bell D., 1965, MNRAS, 130, 125
Goodman J., 2003, MNRAS, 339, 937
Goodman A. A., Benson P. J., Fuller G. A., Myers P. C., 1993, ApJ, 406, 528
Harsono D., Alexander R. D., Levin Y., 2011, MNRAS, 413, 423
Hennebelle P., Ciardi A., 2009, A&A, 506, L29
Kim W.-T., Ostriker E. C., 2001, The Astrophysical Journal, 559, 70
Kim W.-T., Ostriker E. C., Stone J. M., 2003, The Astrophysical Journal, 599, 1157
Kratter K., Lodato G., 2016, ARA&A, 54, 271
Kratter K. M., Murray-Clay R. A., 2011, ApJ, 740, 1
Kratter K. M., Matzner C. D., Krumholz M. R., Klein R. I., 2010, ApJ, 708, 1585
Laughlin G., Rozyczka M., 1996, ApJ, 456, 279
Lin M.-K., 2014, The Astrophysical Journal, 790, 13
Lin D. N. C., Pringle J. E., 1990, ApJ, 358, 515
Lodato G., 2007, Rivista Del Nuovo Cimento, 30, 293
Lodato G., Price D. J., 2010, MNRAS, 405, 1212
Lynden-Bell D., Kalnajs A. J., 1972, MNRAS, 157, 1
Malik M., Meru F., Mayer L., Meyer M., 2015, ApJ, 802, 56
Marti-Vidal I., Muller S., Vlemmings W., Horellou C., Aalto S., 2015, Science, 348, 311
Martin R. G., Lubow S. H., 2014, MNRAS, 437, 682
Maury A. J., et al., 2010, A&A, 512, A40
Meru F., Bate M. R., 2011, MNRAS, 411, L1
Meru F., Bate M. R., 2012, MNRAS, 427, 2022
Michael S., Steiman-Cameron T. Y., Durisen R. H., Boley A. C., 2012, ApJ, 746, 98
Morris J., Monaghan J., 1997, Journal of Computational Physics, 136, 41
Murray J. R., 1996, MNRAS, 279, 402
Nayakshin S., 2010, MNRAS, 408, L36
Paardekooper S.-J., 2012, MNRAS, 421, 3286
Paczynski B., 1978, Acta Astronomica, 28, 91
Price D. J., 2007, PASA, 24, 159
Price D. J., 2012, Journal of Computational Physics, 231, 759
Price D. J., Bate M. R., 2007, MNRAS, 377, 77
Price D. J., Monaghan J. J., 2004a, MNRAS, 348, 123

Price D. J., Monaghan J. J., 2004b, MNRAS, 348, 139
Price D. J., Monaghan J. J., 2005, MNRAS, 364, 384
Pudritz R. E., Hardcastle M. J., Gabuzda D. C., 2012, Space Science Reviews, 169, 27
Rice K., 2016, PASA, 33, id.e012
Rice W. K. M., Lodato G., Pringle J. E., Armitage P. J., Bonnell I. A., 2004, MNRAS, 355, 543
Rice W. K. M., Lodato G., Armitage P. J., 2005, MNRAS, 364, L56
Rice W. K. M., Forgan D. H., Armitage P. J., 2012, MNRAS, 420, 1640
Rice W. K. M., Paardekooper S.-J., Forgan D. H., Armitage P. J., 2014, MNRAS, 438, 1593
Riols A., Latter H., 2016, Monthly Notices of the Royal Astronomical Society, 460, 2223
Rodríguez-Kamenetzky A., Carrasco-González C., Araudo A., Torrelles J. M., Anglada G., Martí J., Rodríguez L. F., Valotto C., 2016, The Astrophysical Journal, 818, 27
Seifried D., Banerjee R., Pudritz R. E., Klessen R. S., 2013, Monthly Notices of the Royal Astronomical Society, 432, 3320
Shakura N. I., Sunyaev R. A., 1973, A&A, 24, 337
Smith R., Clark P., Bonnell I. A., 2009, MNRAS, 396, 830
Springel V., White S., Tormen G., Kauffmann G., 2001, MNRAS, 328, 726
Strittmatter P. A., 1966, Monthly Notices of the Royal Astronomical Society, 131, 491
Tobin J. J., et al., 2015, ApJ, 805, 125
Tobin J. J., et al., 2016, Nature, 538, 483
Tomida K., Okuzumi S., Machida M. N., 2015, ApJ, 801, 117
Toomre A., 1964, ApJ, 139, 1217
Tricco T. S., Price D. J., 2012, Journal of Computational Physics, 231, 7214
Tricco T. S., Price D. J., Bate M. R., 2016, Journal of Computational Physics, 322, 326
Tsukamoto Y., Takahashi S. Z., Machida M. N., Inutsuka S.-i., 2014, MNRAS, 446, 1175
Wurster J., Price D. J., Bate M. R., 2016, MNRAS, 457, 1037
Young M. D., Clarke C. J., 2015, MNRAS, 451, 3987
Young M. D., Clarke C. J., 2016, MNRAS, 455, 1438
Zhu Z., Hartmann L., Nelson R. P., Gammie C. F., 2012, The Astrophysical Journal, 746, 110